# Supporting Information

# Effective defect passivation with a designer ionic molecule for high-efficiency vapour-deposited inorganic phase-pure $CsPbBr_3$ perovskite solar cells

Ruxin Guo,‡[ad] Junmin Xia,‡[b] Hao Gu,‡[b] Yan Zhao,[a] Xuke Chu,[a] Xianghuan Meng,[a] Zhiheng Wu,[ad] Jiangning Li,[a] Yanyan Duan,[a] Zhenzhen Li,[a] Zhaorui Wen,[b] Shi Chen,[b] Yongqing Cai,[b] Chao Liang,*[c] Yonglong Shen,*[ad] Guichuan Xing,*[b] Wei Zhang[e] and Guosheng Shao*[ad]

[a]State Centre for International Cooperation on Designer Low-carbon & Environmental Materials (CDLCEM), School of Materials Science and Engineering, Zhengzhou University, Zhengzhou 450001, P. R. China.
[b]Joint Key Laboratory of the Ministry of Education Institute of Applied Physics and Materials Engineering University of Macau Avenida da Universidade Taipa, Macau 999078, P. R. China.
[c]MOE Key Laboratory for Nonequilibrium Synthesis and Modulation of Condensed Matter, School of Physics, Xi'an Jiaotong University, Xi'an 710049, P. R. China.
[d]Zhengzhou Materials Genome Institute (ZMGI), Building 2, Zhongyuanzhigu, Xingyang, Zhengzhou 450100, P. R. China.
[e]Advanced Technology Institute (ATI), University of Surrey, Guildford, Surrey, GU27XH, UK.
‡These authors contributed equally.

Email: chaoliang@um.edu.mo, shenyonglong@zzu.edu.cn, gcxing@um.edu.mo; gsshao@zzu.edu.cn

**Supplementary Figures**

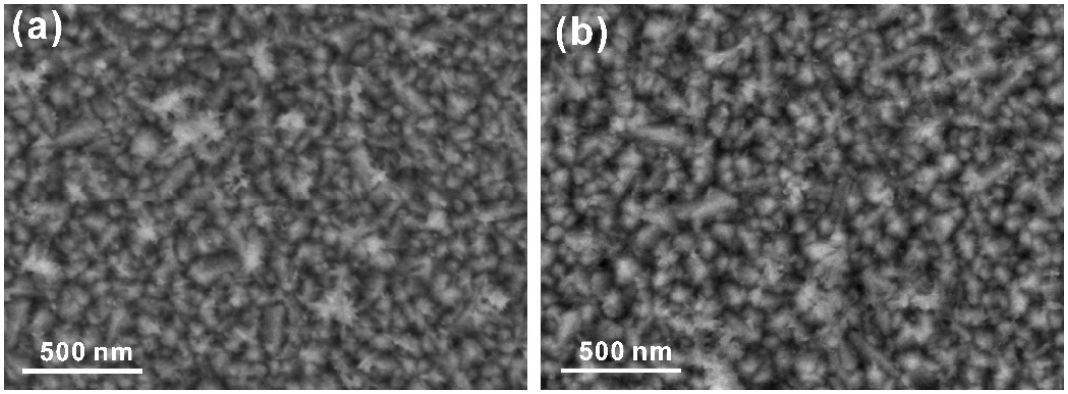


**Fig. S1** The top-view of (a) $TiO_2$ and (b) $TiO_2$/DTPT films deposited on glass/FTO.

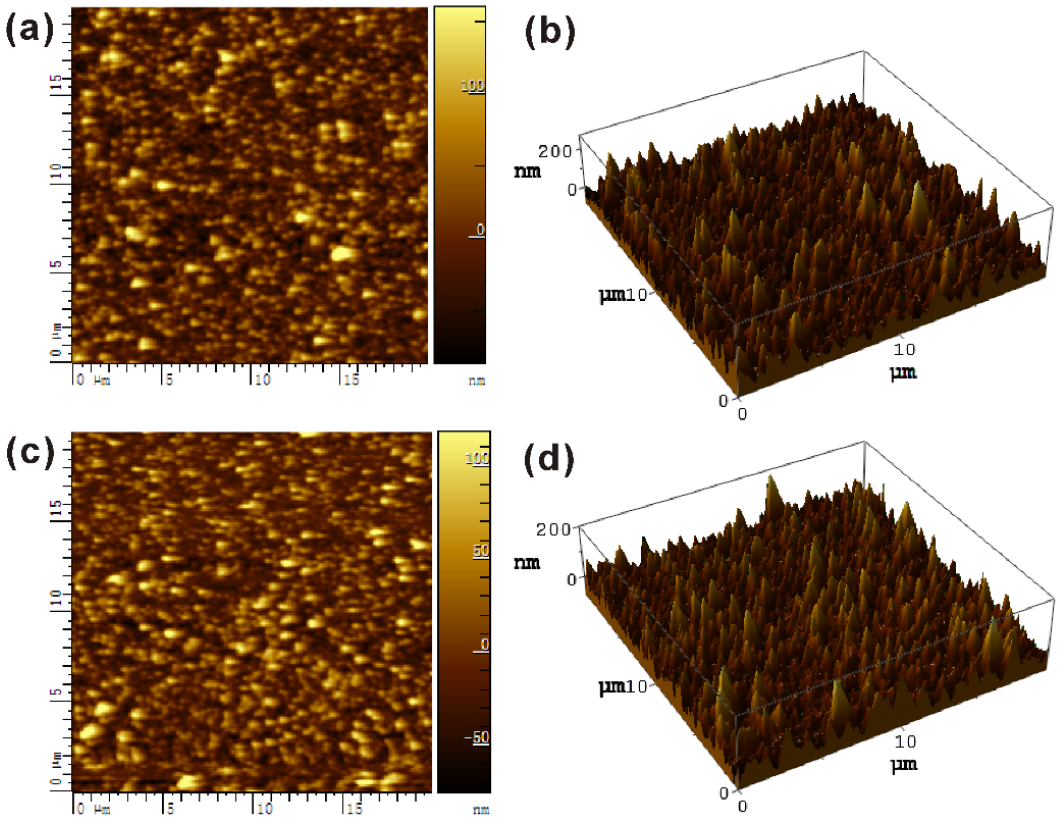


**Fig. S2** AFM pictures of (a) $TiO_2$ and (c) $TiO_2$/DTPT films, corresponding 3D diagram.

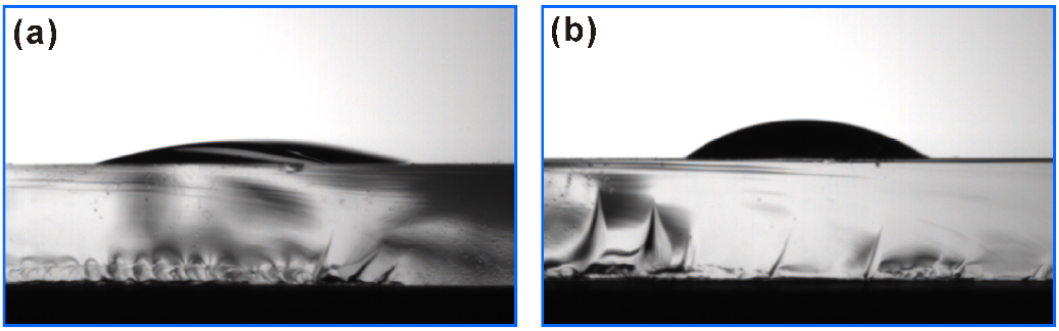


**Fig. S3** The images show contact angle measurement of water and on (a) $TiO_2$ and (b) $TiO_2$/DTPT films.

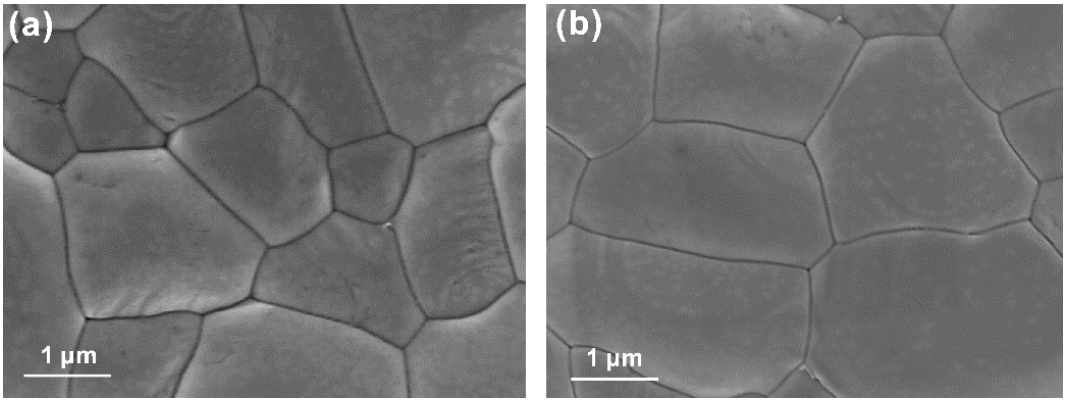


**Fig. S4** Top view SEM images of $CsPbBr_3$ films based on (a) $TiO_2$ and (b) $TiO_2$/DTPT films.

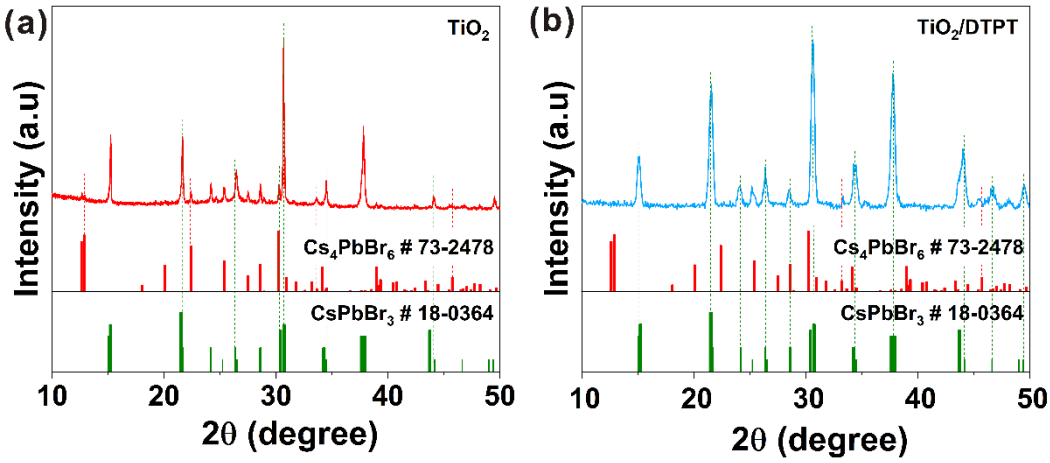


**Fig. S5** XRD patterns of $CsPbBr_3$ films based on (a) $TiO_2$ and (b) $TiO_2$/DTPT films.

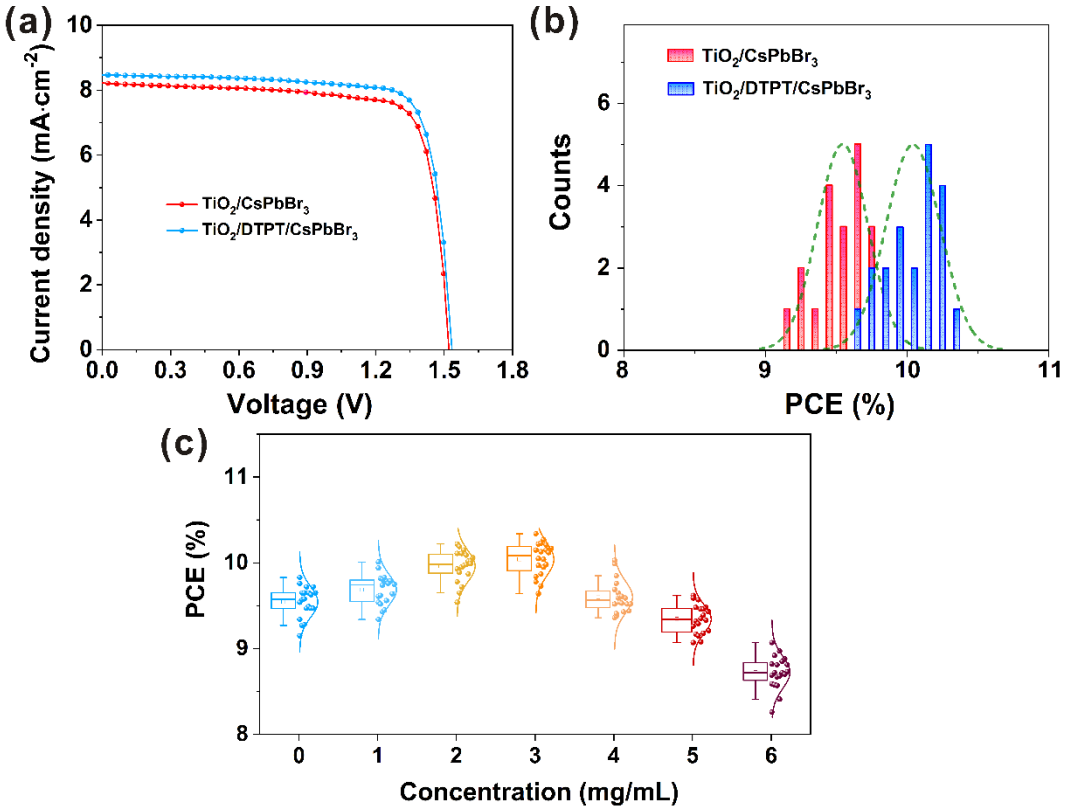


**Fig. S6** (a) The *J-V* curves of PSCs and (b) histograms of PCEs measured (40 devices) based on $TiO_2$ and $TiO_2$/DTPT films. (c) The PCE statistics of devices for each DTPT concentrations deposited on $TiO_2$ films.

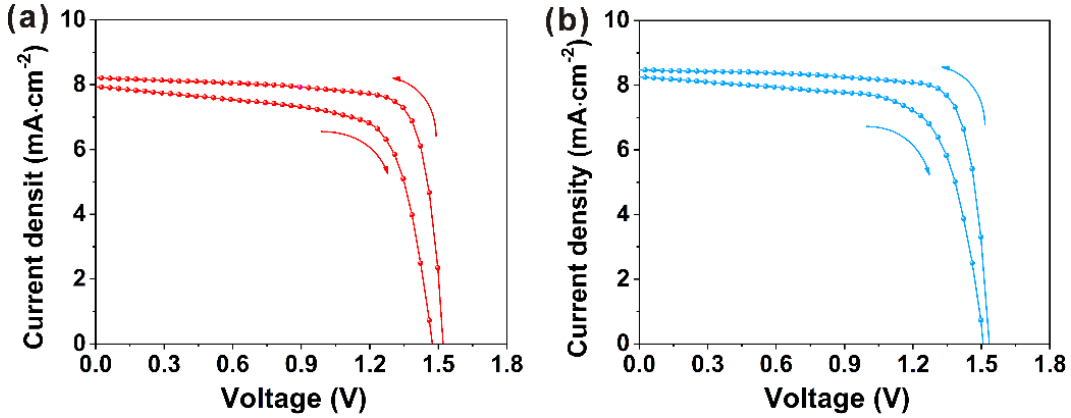


**Fig. S7** Reverse scan and forward scan *J-V* curves of PSCs based on (a) $TiO_2$ and (b) $TiO_2$/DTPT films.

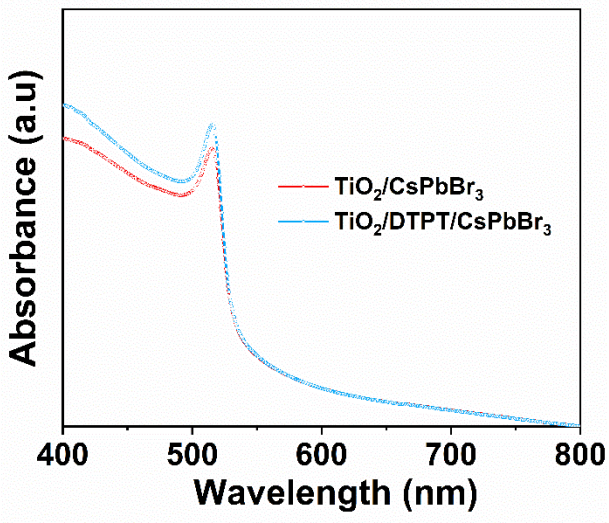


**Fig. S8** Absorption spectra of $CsPbBr_3$ films deposited on $TiO_2$ and $TiO_2$/DTPT films.

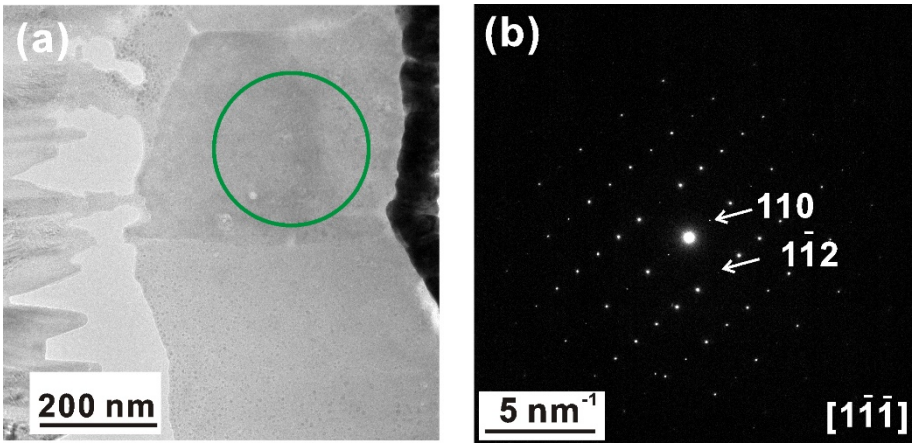


**Fig. S9** (a) Cross-section TEM image of $CsPbBr_3$ film with DTPT treated and (b) its SAED in green circle in the TEM image.

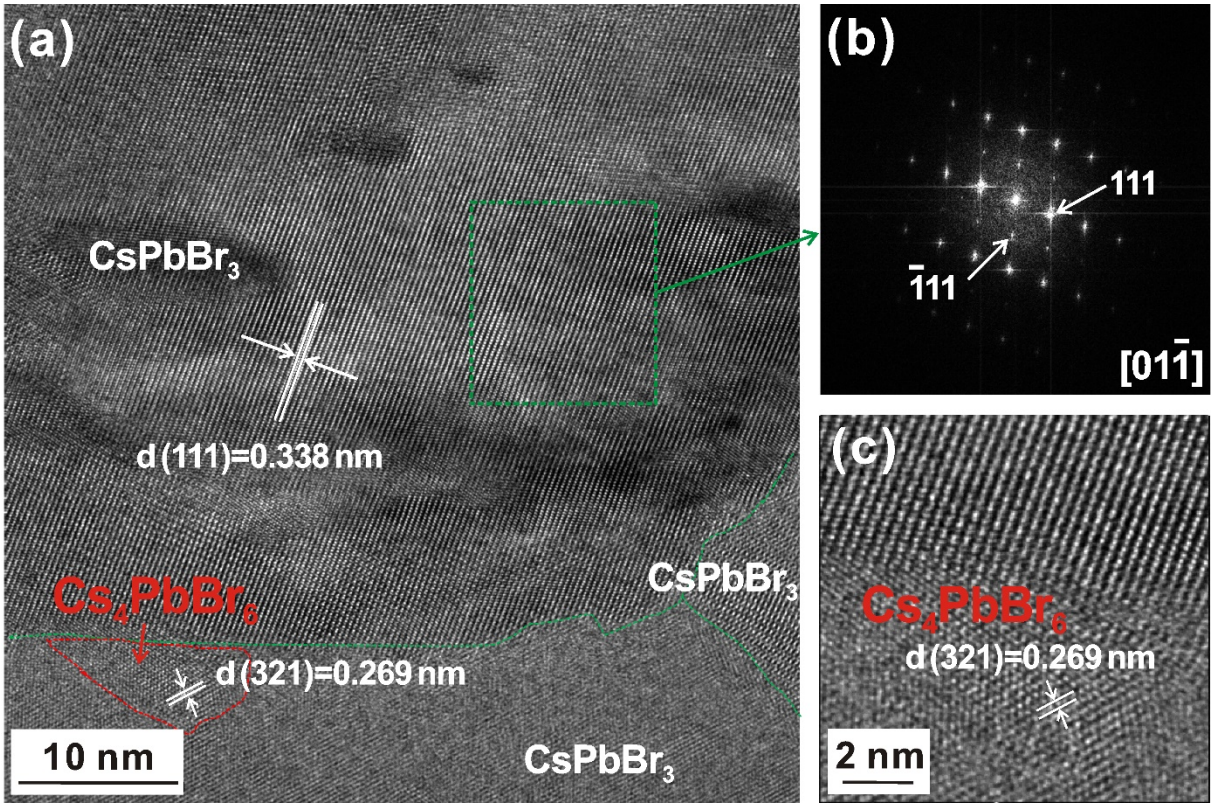


**Fig. S10** (a) Planar-view high-resolution transmission electron microscopy (HRTEM) image, (b) FFT and (c) Partial enlargement image of $TiO_2$/DTPT/$CsPbBr_3$ film without top-surface DTPT treated.

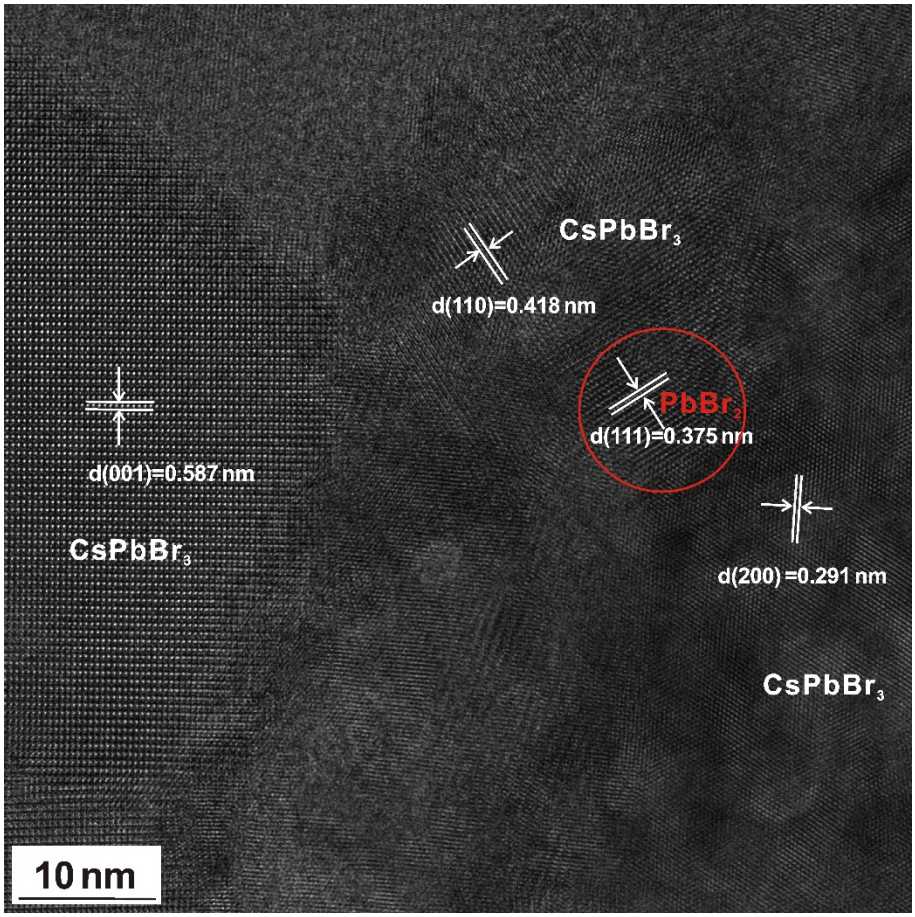


**Fig. S11** Planar-view HRTEM image of $TiO_2$/DTPT/$CsPbBr_3$ film without top-surface DTPT treated.

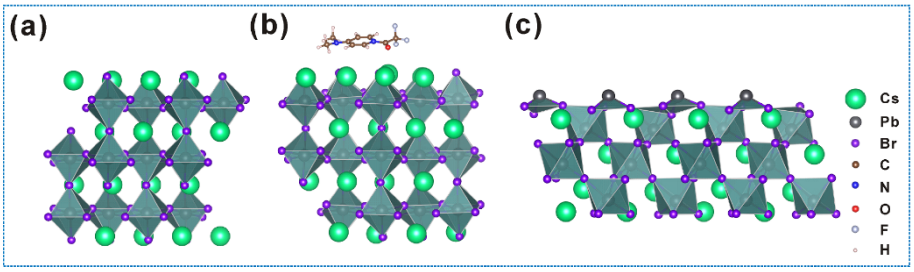


**Fig. S12** The structures without and with DTPT on the surface. The (001) phase of $CsPbBr_3$ (a) without and (b) with DTPT on the surface; (c) The (110) phase of $CsPbBr_3$ without DTPT on the surface.

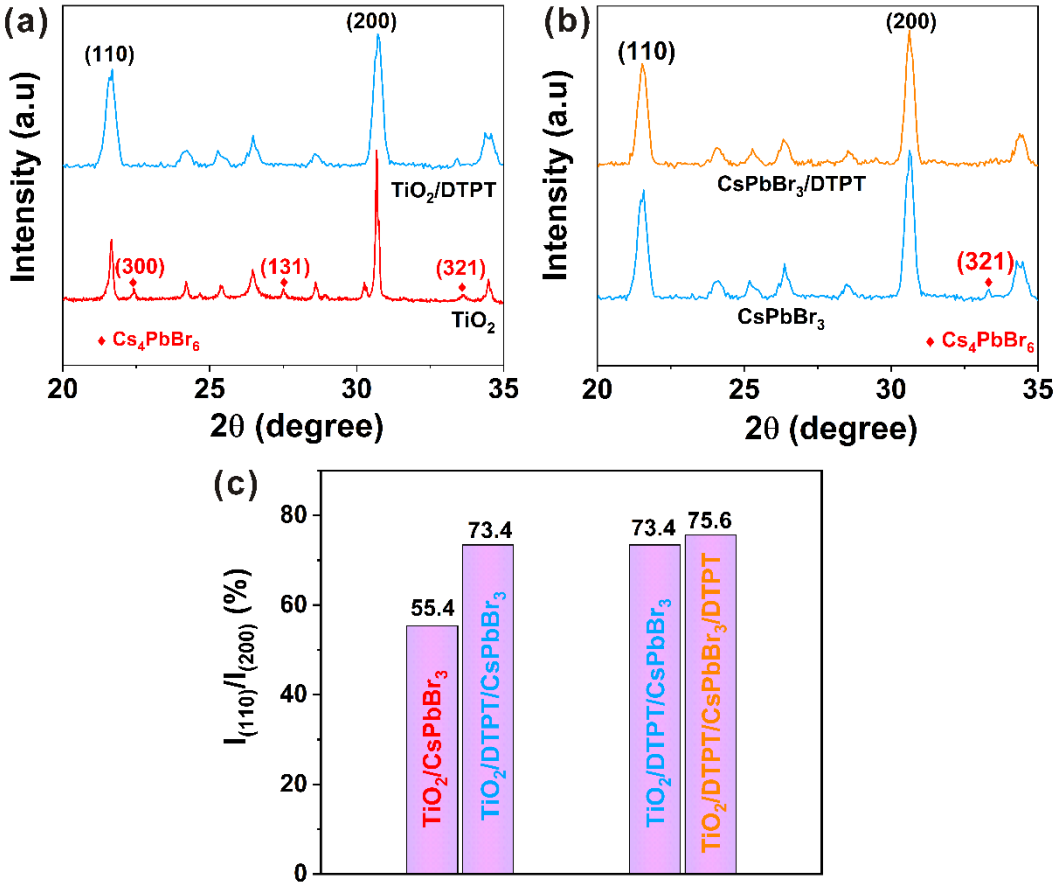


**Fig. S13** The enlarged XRD spectra of $CsPbBr_3$ films deposited on (a) $TiO_2$ and $TiO_2$/DTPT films and (b) $CsPbBr_3$ and $CsPbBr_3$/DTPT substrates; (c) The peak intensity ratio of (110) and (200) in $TiO_2$/ $CsPbBr_3$, $TiO_2$/DTPT/$CsPbBr_3$ and $TiO_2$/DTPT/$CsPbBr_3$/DTPT films.

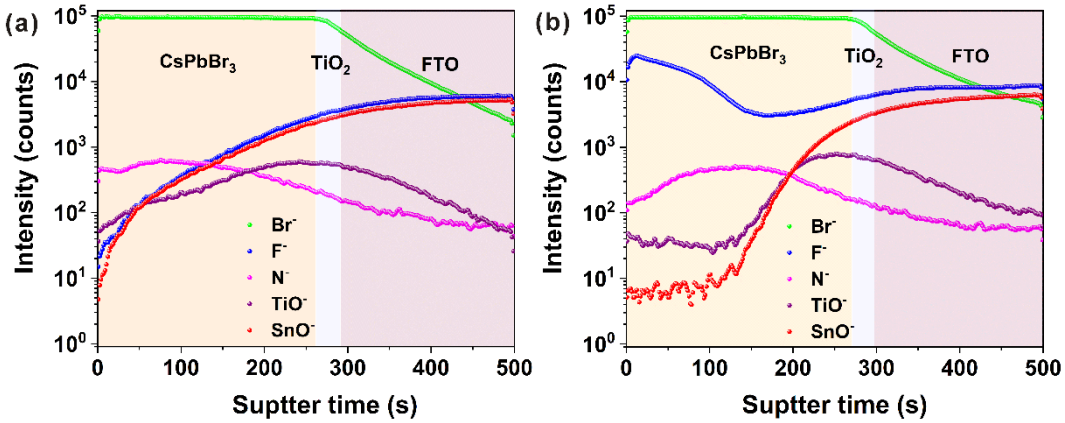


**Fig. S14** ToF-SIMS depth profiles of the (a) $CsPbBr_3$ and (b) $CsPbBr_3$/DTPT films.

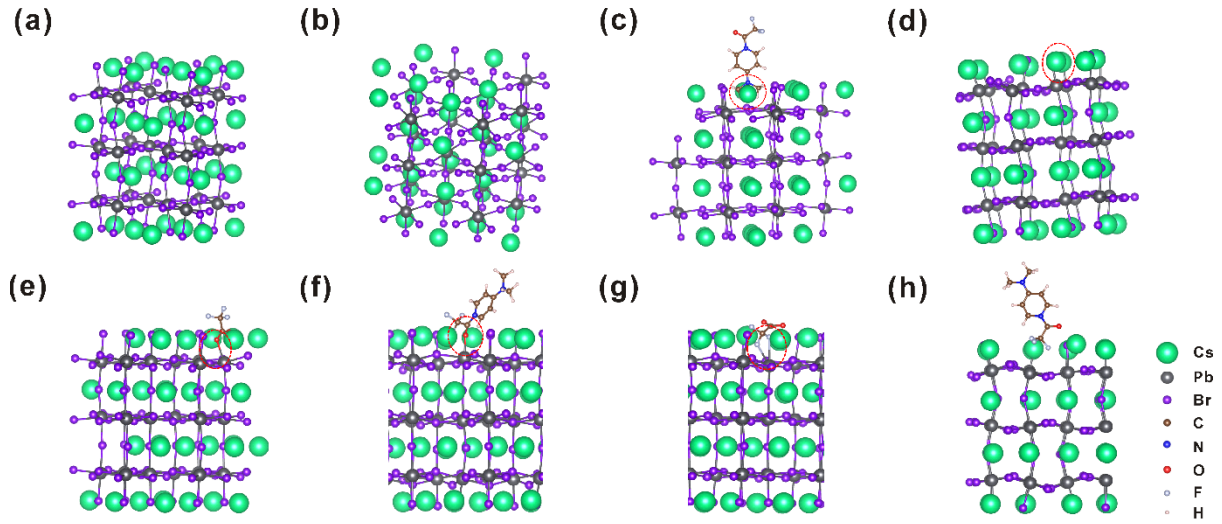


**Fig. S15** The structures of the $CsPbBr_3$ with vacancies and passivated. (a) The pristine; (b) with $V_{CS}$; (c) $V_{CS}$ passivated by the DTPT; (d) with $V_{Br}$; (e) $V_{Br}$ passivated by the carboxylic acid group in $CF_3COO^-$; (f) $V_{Br}$ passivated by the C=O in DTPT; (g) $V_{Br}$ passivated by the $CF_3$- group in $CF_3COO^-$; (h) $V_{Br}$ passivated by $CF_3$- group in DTPT.

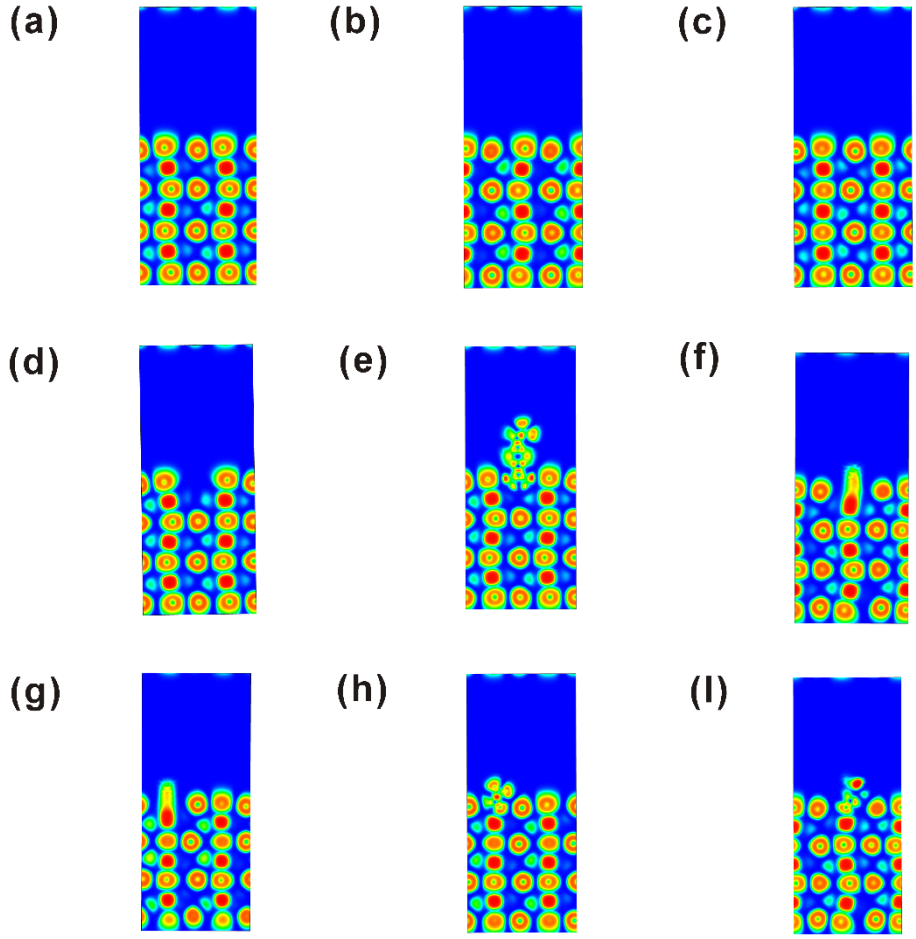


**Fig. S16** Electron localization function (ELF) results of the $CsPbBr_3$ with vacancies and passivated. (a) 2D section (0 0.33 0) of the pristine $CsPbBr_3$; (b) 2D section (0 0.5 0) of the pristine $CsPbBr_3$; (c) 2D section (0.5 0 0) of the pristine $CsPbBr_3$; (d) 2D section (0 0.5 0) of the $CsPbBr_3$ with $V_{Cs}$; (e) 2D section (0 0.5 0) of the DTPT passivated $CsPbBr_3$ with $V_{Cs}$; (f) 2D section (0 0.33 0) of the $CsPbBr_3$ with $V_{Br}$; (g) 2D section (0 0.5 0) of the $CsPbBr_3$ with $V_{Br}$; (h) 2D section (0 0.33 0) of the $CF_3COO^-$ passivated $CsPbBr_3$ with $V_{Br}$; (i) 2D section (0 0.5 0) of the DTPT passivated $CsPbBr_3$ with $V_{Br}$.

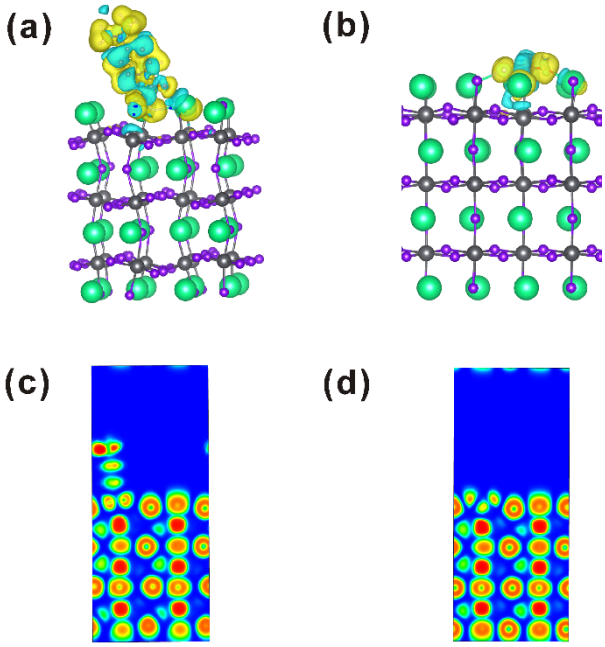


**Fig. S17** The DFT result of the $CsPbBr_3$ with $V_{Br}$ passivated by the $CF_3$- group of DTPT. Differential charge density for (a) $V_{Br}$ passivated by the $CF_3$- group in DTPT and (b) $V_{Br}$ passivated by the $CF_3$- group in $CF_3COO^-$; ELF results for (c) $V_{Br}$ passivated by the $CF_3$- group in DTPT and (d) $V_{Br}$ passivated by the $CF_3$- group in $CF_3COO^-$.

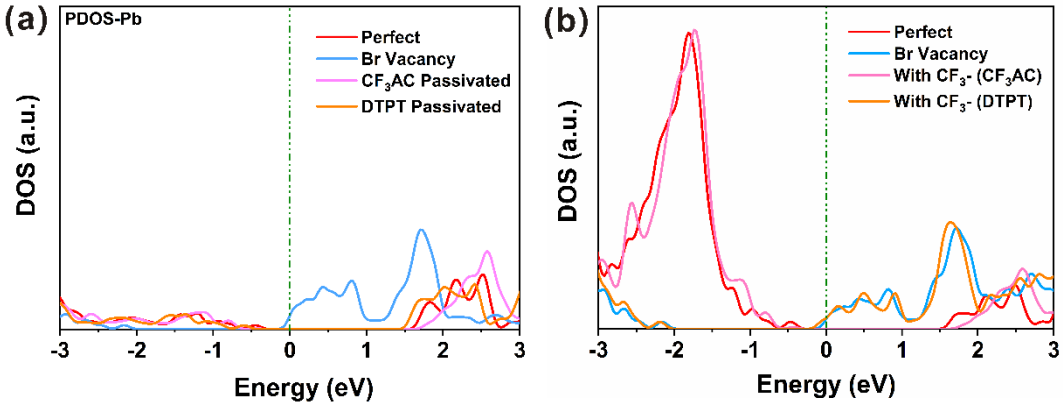


**Fig. S18** Electronic partial density of state (PDOS) curves for Pb of the $CsPbBr_3$ with $V_{Br}$ passivated by $CF_3AC$ and DTPT; (b) Density of state of $CsPbBr_3$ with $V_{Br}$ passivated by the $CF_3$- group of $CF_3AC$ and DTPT.

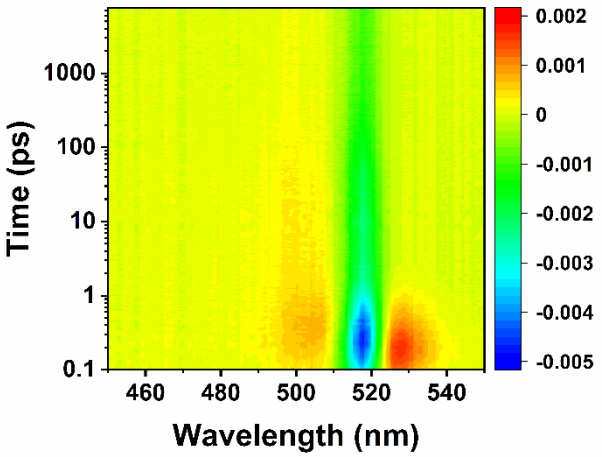


**Fig. S19** Pseudo-colour femtosecond transient absorption (fs-T(A) spectrum plots of $CsPbBr_3$ film upon a pulsed fs-laser excitation at 400 nm.

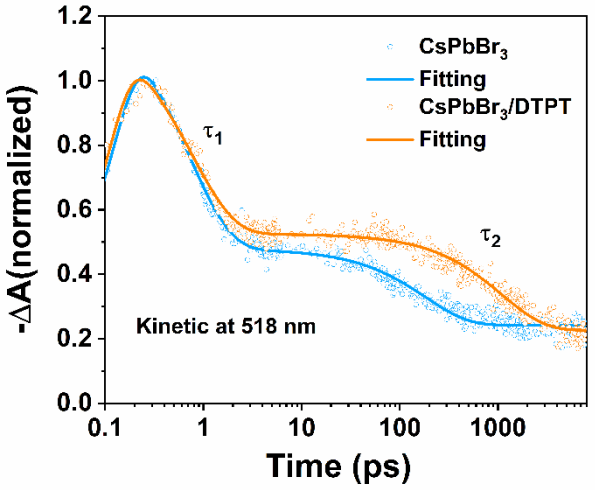


**Fig. S20** Normalized bleaching kinetics at 518 nm of the $CsPbBr_3$ and $CsPbBr_3$/DTPT films.

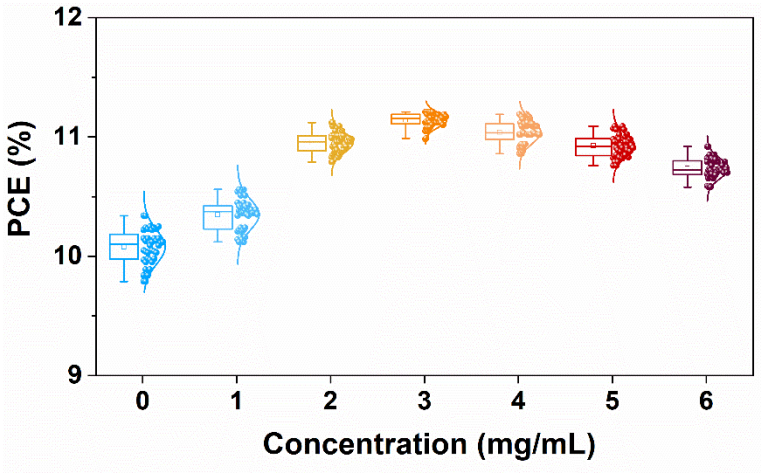


**Fig. S21** The PCE statistics of 40 devices for each DTPT concentrations.

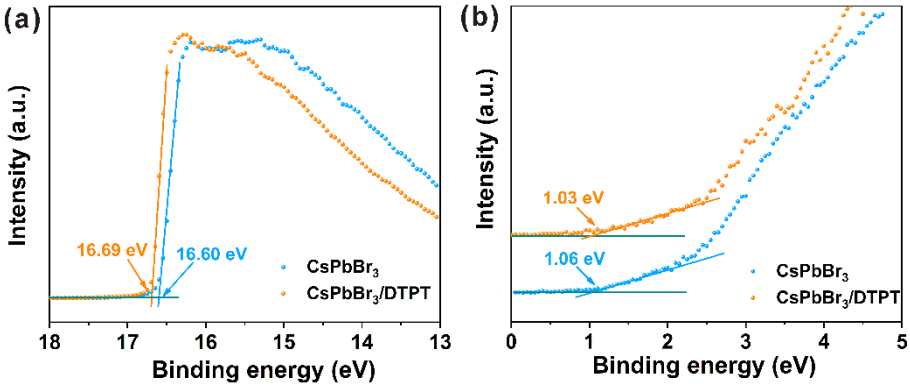


**Fig. S22** (a) The cut-off energy ($E_{cut\text{-}off}$), (b) valence band maximum (VBM) edges of $CsPbBr_3$ and $CsPbBr_3$/DTPT films.

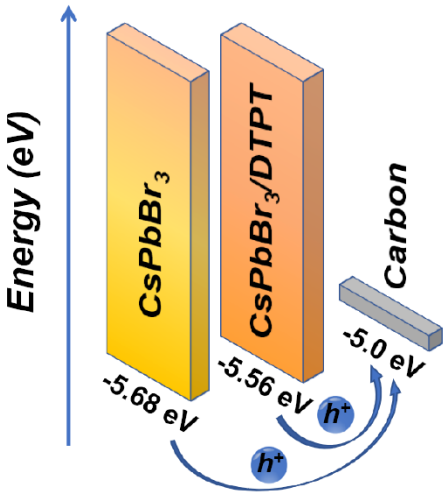


**Fig. S23** Energy band of each isolated layer in the device.

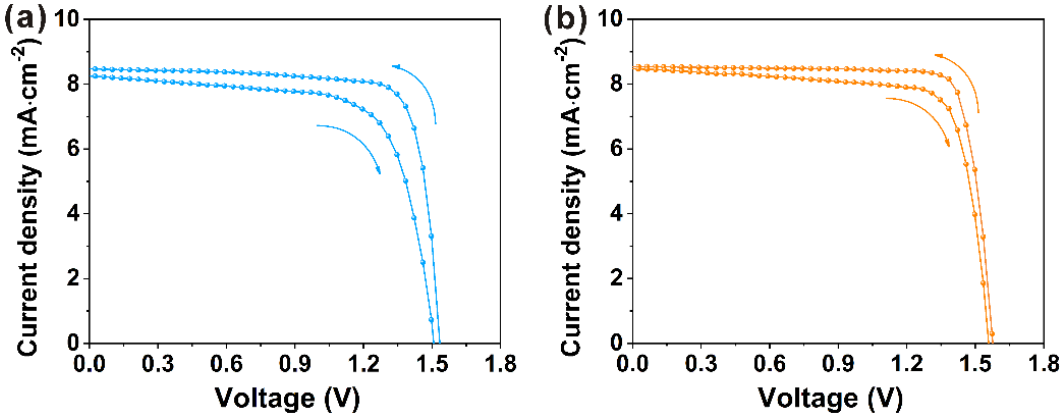


**Fig. S24** The *J-V* curves of PSCs based on (a) $CsPbBr_3$ and (b) $CsPbBr_3$/DTPT under different scanning directions.

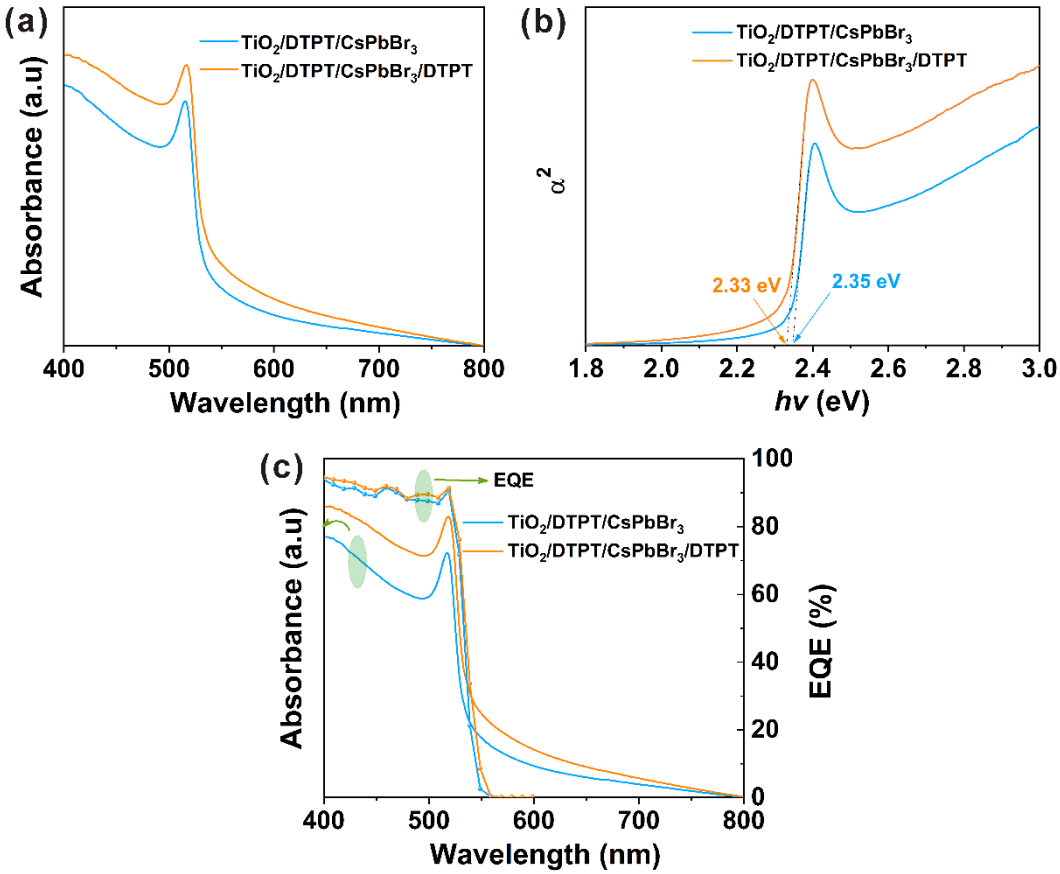


**Fig. S25** (a) Absorption spectra and (b) Tauc plots of $CsPbBr_3$ and $CsPbBr_3$/DTPT films deposited on $TiO_2$/DTPT films. (c) Absorption spectra and EQE spectra of $CsPbBr_3$ and $CsPbBr_3$/DTPT films deposited on $TiO_2$/DTPT films.

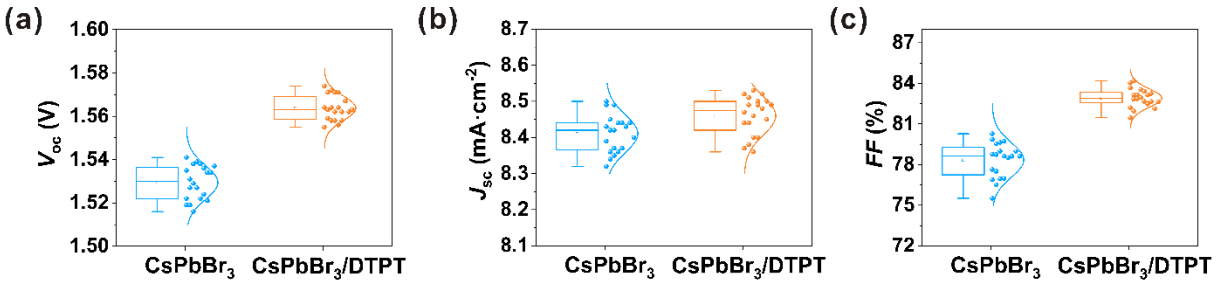


**Fig. S26** Statistical (a) $V_{oc}$, (b) $J_{sc}$, and (c) *FF* of the devices with and without DTPT.

## Supplementary Tables

**Table S1.** Photovoltaic parameters of PSCs based on $TiO_2$ and $TiO_2$ /DTPT films.

| Samples | Scan-direction | PCE (%) | $V_{oc}$ (V) | $J_{sc}$ ($mA \cdot cm^{-2}$) | *FF* (%) |
|---|---|---|---|---|---|
| $TiO_2$ | backward | 9.83 | 1.521 | 8.22 | 78.66 |
| | forward | 8.19 | 1.475 | 7.94 | 69.93 |
| $TiO_2$/DTPT | backward | 10.34 | 1.535 | 8.43 | 79.87 |
| | forward | 8.71 | 1.508 | 8.23 | 70.18 |

**Table S2.** Photovoltaic parameters of PSCs based on $CsPbBr_3$ and $CsPbBr_3$/DTPT.

| Samples | Scan-direction | PCE (%) | $V_{oc}$ (V) | $J_{sc}$ ($mA \cdot cm^{-2}$) | *FF* (%) |
|---|---|---|---|---|---|
| $CsPbBr_3$ | backward | 10.34 | 1.535 | 8.43 | 79.87 |
| | forward | 8.71 | 1.508 | 8.23 | 70.18 |
| $CsPbBr_3$/DTPT | backward | 11.21 | 1.574 | 8.52 | 83.67 |
| | forward | 10.12 | 1.559 | 8.47 | 76.64 |

**Table S3**. Comparison of photovoltaic parameters for state-of-the-art $CsPbBr_3$ PSCs.

| PSCs | PCE (%) | $J_{sc}$ (mA cm$^{-2}$) | $V_{oc}$ (V) | *FF* (%) | Ref. |
|---|---|---|---|---|---|
| FTO/$TiO_2$/DTPT/$CsPbBr_3$/DTPT/Carbon | 11.21 | 8.52 | 1.574 | 83.67 | This work |
| FTO/$SnO_2$-$TiO_xCl_{4-2x}$/$CsPbBr_3$+ $Ti_3C_2Cl_x$/$Ti_3C_2Cl_x$/Carbon | 11.08 | 7.87 | 1.702 | 82.7 | 1 |
| FTO/c-$TiO_2$/m-$TiO_2$/$CsPbBr_3$/ $CuInS_2$/ZnS QDs/LPP-Carbon | 10.85 | 7.73 | 1.626 | 86.3 | 2 |
| FTO/*c*-$TiO_2$/*m*-$TiO_2$/GQDs/$CsPbBr_3$/Carbon | 9.72 | 8.12 | 1.458 | 82.1 | 3 |
| FTO/c-$TiO_2$/m-$TiO_2$/$Sm^{3+}$-$CsPbBr_3$/ Cu(Cr,Ba)$O_2$/Carbon | 10.79 | 7.81 | 1.615 | 85.5 | 4 |
| FTO/c-$TiO_2$/m-$TiO_2$/$Sm^{3+}$-$CsPbBr_3$/Carbon | 10.14 | 7.48 | 1.594 | 85.1 | 5 |
| FTO/c-$TiO_2$/m-$TiO_2$/GQDs/$CsPbBr_3$/MnS/Carbon | 10.45 | 8.28 | 1.52 | 83 | 6 |
| FTO/c-$TiO_2$/m-$TiO_2$/$CsPbBr_3$/P1Z1/Carbon | 10.03 | 7.652 | 1.578 | 83.06 | 7 |
| FTO/c-$TiO_2$/PTI-$CsPbBr_3$/spiro-OMeTAD/Ag | 10.91 | 9.78 | 1.498 | 74.47 | 8 |
| FTO/c-$TiO_2$/$CsPbBr_3$/$CsPbBr_3$-$CsPb_2Br_5$/$CsPbBr_3$-$Cs_4PbBr_6$/Carbon | 10.17 | 9.26 | 1.461 | 75.39 | 9 |
| FTO/c-$TiO_2$/$CsPbBr_3$/Carbon | 9.35 | 7.37 | 1.545 | 82.2 | 10 |
| FTO/c-$TiO_2$/m-$TiO_2$/ $CsPb_{0.97}Tb_{0.03}Br_3$/SnS:ZnS/$NiO_x$/carbon | 10.26 | 8.21 | 1.57 | 79.6 | 11 |
| FTO/$SnO_2$/$CsPbBr_3$/N-CQDs/Carbon | 10.71 | 7.87 | 1.622 | 80.1 | 12 |
| FTO/$SnO_2$/$CsPbBr_3$/$CsSnBr_3$/Carbon | 10.60 | 7.80 | 1.610 | 84.4 | 13 |
| FTO/$SnO_2$-$TiO_xCl_{4-2x}$/$WS_2$/$CsPbBr_3$/Carbon | 10.65 | 7.95 | 1.70 | 79 | 14 |
| FTO/*c*-$TiO_2$/$CsPbBr_3$–$CsPb_2Br_5$/spiro-OMeTAD/Ag | 8.34 | 8.48 | 1.296 | 75.9 | 15 |
| FTO/c-$TiO_2$/m-$TiO_2$/$CsPbBr_{2.98}Cl_{0.02}$/Carbon | 9.73 | 7.47 | 1.571 | 82.93 | 16 |

**Table S4**. Comparison of photovoltaic parameters for large-area $CsPbBr_3$ PSCs.

| PSCs | Active area | Method | PCE (%) | $J_{sc}$ (mA $cm^{-2}$) | $V_{oc}$ (V) | *FF* (%) | Ref. |
|---|---|---|---|---|---|---|---|
| FTO/$TiO_2$/DTPT/$CsPbBr_3$/DTPT/Carbon | 1 $cm^2$ | Vapour deposition | 9.18 | 7.81 | 1.509 | 77.85 | This work |
| FTO/c-$TiO_2$/$CsPbBr_3$/ spiro-OMeTAD/Au | 1 $cm^2$ | Vacuum evaporation | 5.37 | 5.11 | 1.32 | 79.32 | [17] |
| FTO/c-$TiO_2$/ $CsPbBr_3$/CuPc/Carbon | 1 $cm^2$ | Vacuum evaporation | 6.21 | 6.65 | 1.375 | 67.9 | [18] |
| FTO/c-$TiO_2$/$SnO_2$/ $CsPbBr_3$/CuPc/carbon | 1 $cm^2$ | Spin-coating | 6.9 | 6.93 | 1.396 | 71.3 | [19] |
| FTO/Ga-$SnO_2$/ $CsPbBr_3$/Carbon | 1 $cm^2$ | Spin-coating | 5.98 | 7.58 | 1.311 | 60.2 | [20] |
| FTO/c-$TiO_2$/m-$TiO_2$/$Cs_{0.91}Rb_{0.09}PbBr_3$/ Carbon | 1 $cm^2$ | Spin-coating | 7.07 | — | — | — | [21] |

## Supplementary References


1 Q. Zhou, J. Duan, J. Du, Q. Guo, Q. Zhang, X. Yang, Y. Duan and Q. Tang, *Adv. Sci.*, 2021, **8**, 2101418.
2 J. Duan, Y. Wang, X. Yang and Q. Tang, *Angew. Chem. Int. Ed.*, 2020, **59**, 4391-4395.
3 J. Duan, Y. Zhao, B. He and Q. Tang, *Angew. Chem. Int. Ed.*, 2018, **57**, 3787-3791.
4 J. Duan, Y. Zhao, Y. Wang, X. Yang, Q. Tang, *Angew. Chem. Int. Ed.*, 2019, **58**, 16147-16151.
5 J. Duan, Y. Zhao, X. Yang, Y. Wang, B. He and Q. Tang, *Adv. Energy Mater.*, 2018, **8**, 1802346.
6 X. Li, Y. Tan, H. Lai, S. Li, Y. Chen, S. Li, P. Xu and J. Yang, *ACS Appl. Mater. Interfaces*, 2019, **11**, 29746-29752.
7 Y. Liu, B. He, J. Duan, Y. Zhao, Y. Ding, M. Tang, H. Chen and Q. Tang, *J. Mater. Chem. A*, 2019, **7**, 12635-12644.
8 G. Tong, T. Chen, H. Li, L. Qiu, Z. Liu, Y. Dang, W. Song, L. K. Ono, Y. Jiang and Y. Qi, *Nano Energy*, 2019, **65**, 104015.
9 G. Tong, T. Chen, H. Li, W. Song, Y. Chang, J. Liu, L. Yu, J. Xu, Y. Qi and Y. Jiang, *Sol. RRL*, 2019, **3**, 1900030.
10 T. Xiang, Y. Zhang, H. Wu, J. Li, L. Yang, K. Wang, J. Xia, Z. Deng, J. Xiao, W. Li, Z. Ku, F. Huang, J. Zhong, Y. Peng and Y.-B. Cheng, *Sol. Energy Mater. Sol. Cells*, 2020, **206**, 110317.
11 H. Yuan, Y. Zhao, J. Duan, Y. Wang, X. Yang and Q. Tang, *J. Mater. Chem. A*, 2018, **6**, 24324-24329.
12 Y. Zhao, J. Duan, Y. Wang, X. Yang and Q. Tang, *Nano Energy*, 2020, **67**, 104286.
13 Y. Zhao, J. Duan, H. Yuan, Y. Wang, X. Yang, B. He and Q. Tang, *Sol. RRL*, 2019, **3**, 1800284.
14 Q. Zhou, J. Duan, X. Yang, Y. Duan and Q. Tang, *Angew. Chem. Int. Ed.*, 2020, **59**, 21997-22001.
15 H. Li, G. Tong, T. Chen, H. Zhu, G. Li, Y. Chang, L. Wang and Y. Jiang, *J. Mater. Chem. A*, 2018, **6**, 14255-14261.
16. X. Li, B. He, Z. Gong, J. Zhu, W. Zhang, H. Chen, Y. Duan and Q. Tang, *Sol. RRL*, 2020, **4**, 2000362.
17. J. Lei, F. Gao, H. Wang, J. Li, J. Jiang, X. Wu, R. Gao, Z. Yang and S. Liu, *Sol. Energy Mater. Sol. Cells*, 2018, **187**, 1-8.
18. X. Liu, X. Tan, Z. Liu, B. Sun, J. Li, S. Xi, T. Shi and G. Liao, *J. Power Sources*, 2019, **443**, 227269.
19. X. Liu, X. Tan, Z. Liu, H. Ye, B. Sun, T. Shi, Z. Tang and G. Liao, *Nano Energy*, 2019, **56**, 184-195.
20. Y. Zhao, Q. Deng, R. Guo, Z. Wu, Y. Li, Y. Duan, Y. Shen, W. Zhang and G. Shao, *ACS Appl. Mater. Interfaces*, 2020, **12**, 54904-54915.
21. Y. Li, J. Duan, H. Yuan, Y. Zhao, B. He and Q. Tang, *Sol. RRL*, 2018, **2**, 1800164.